Emergence of Geometrical Optical Nonlinearities in Photonic Crystal Fiber Nanowires

Fabio Biancalana, Truong X. Tran, Sebastian Stark, Markus A. Schmidt, and Philip St. J. Russell

Max Planck Institute for the Science of Light, Günther-Scharowsky Strasse 1, Bau 26, 91058 Erlangen, Germany

(Received 19 February 2010; revised manuscript received 30 July 2010; published 27 August 2010)

We demonstrate analytically and numerically that a subwavelength-core dielectric photonic nanowire embedded in a properly designed photonic crystal fiber cladding shows evidence of a previously unknown kind of nonlinearity (the magnitude of which is strongly dependent on the waveguide parameters) which acts on solitons so as to considerably reduce their Raman self-frequency shift. An explanation of the phenomenon in terms of indirect pulse negative chirping and broadening is given by using the moment method. Our conclusions are supported by detailed numerical simulations.

DOI: 10.1103/PhysRevLett.105.093904 PACS numbers: 42.65.Tg

Photonic nanowires (PNs), i.e., dielectric waveguides with a subwavelength core diameter, tight mode confinement, and strong waveguide dispersion, have recently attracted growing interest due to accessibility of new fabrication techniques for a large variety of materials, which may lead to a number of miniaturized, high-performance photonic devices [1]. The small effective modal area exhibited by PNs, which increases considerably the Kerr nonlinear coefficient, and the degree of controllability of the dispersion characteristics, makes PNs especially suitable for the investigation of extreme nonlinear phenomena such as supercontinuum generation, as many optical solitons can be excited by using small pump energies [2].

In recent theoretical work, a novel propagation equation that accurately describes the nonlinear evolution of light pulses in PNs was introduced [3]; see also Eq. (2) of this Letter. The fundamental feature found in [3] is that, thanks to the fact that the correct equation takes into full account the variations in the linear mode profiles of the waveguide with wavelength, new nonlinear effects arise in PNs, unknown in previous formulations based on the generalized nonlinear Schrödinger equation (GNLSE) [4], which all assume fixed transverse field profiles. Most of the additional terms described in Ref. [3] have been found to have an extremely small magnitude, so that they can be safely neglected for large core fibers. However, the longitudinal component of the electric field of the fundamental mode of PNs becomes progressively more important when decreasing the core diameter or when increasing the refractive index contrast between core and cladding [3]. This vigorously breaks the rotational symmetry of the mode, whose transverse profile becomes very sensitive to frequency, thus making the new *geometrical nonlinearity*—as we shall call it in the following—extremely important. In fact, for small enough core sizes, such new nonlinear terms may even enter into strong competition with the Raman effect term for some range of frequencies.

Only the circular geometry for PNs has been considered in Ref. [3]. Circular strands of high-refractive index materials in air or in a homogeneous cladding, however, are far from optimal for experimentally detecting the effects of the novel term, because the maximum of the geometrical nonlinear coefficient is located, as a rule, far away in a region of strong normal dispersion, where bright solitons cannot exist. In fact, as has been anticipated in Ref. [3], the new nonlinearity is visible only in the presence of solitons, and its effects are nearly invisible in the normal dispersion regime.

However, one is by no means restricted to the use of a homogeneous cladding around the high-index core. In this Letter we explore the possibility of introducing the PN into a silica-based photonic crystal fiber (PCF, [5]) with a triangular arrangement of the holes [see Fig. 1(a)]. We call such a design a *photonic crystal fiber nanowire* (PCF NW). Such a structure has the additional advantage that relatively long PNs can be supported by the robust PCF cladding [5,6]. In this Letter we demonstrate that, by means of careful choice of parameters in the design of PCF NWs, one can move the maximum of the geometrical nonlinearity *inside* the region of anomalous dispersion. This will make it much easier to observe the new geometrical nonlinearity experimentally, in that it causes considerable suppression of the soliton self-frequency shift (SSFS, see Ref. [7]) from the very start of the propagation. Thus, just a judicious choice of the geometry of the PCF cladding around the nanowire, which affects the dispersive properties of the waveguide and the way the mode profiles change with wavelength, will be sufficient for the emergence of previously invisible nonlinear effects, thus introducing novel ways of controlling the nonlinear light-matter interactions in the medium, a feat that would be extremely difficult if not impossible to achieve with other simpler geometries.

The fiber geometry that we propose in this Letter is shown in Fig. 1(a). It is made of a silica PCF cladding with a triangular lattice of air holes, with pitch $\Lambda = 1.4\ \mu$m and hole radius $R = 0.56\ \mu$m. The central core, of radius $R_c = 0.5\ \mu$m, is made of a high-refractive index tellurite glass (T2 composition taken from Ref. [8]), which possesses an estimated nonlinear coefficient $n_2 \sim 4 \times 10^{-19}\ \mathrm{m}^{-1}\,\mathrm{W}^{-1}$, almost 15 times larger than that of fused

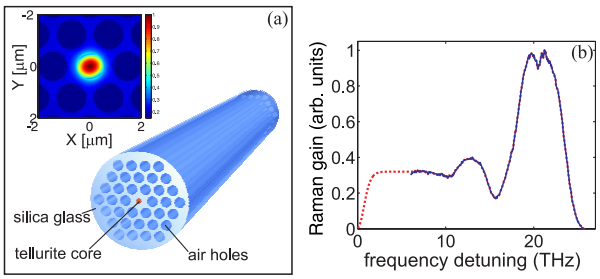

FIG. 1 (color online). (a) Schematics of the proposed PCF nanowire geometry. The central nanowire core is made of tellurite glass ($77TeO_2$-$10Na_2O$-10ZnO-3PbO composition, T2 glass from Ref. [8]), while the cladding is made of silica with a triangular lattice of air holes. Parameters are pitch $\Lambda = 1.4$ μm, hole radius $R = 0.56$ μm, core radius $R_c = 0.5$ μm. Inset: The density plot of the mode profile intensity $||\hat{\mathbf{e}}(\mathbf{r}_\perp)||^2$ of the waveguide for $\lambda = 1.55$ μm is shown. (b) Profile of the Raman gain spectrum for the T2 composition. Solid blue line, experimental data taken from Ref. [8]; dotted red line, fit used in our simulations.

silica [9]. Its Raman gain spectrum $h(\omega)$ is shown in Fig. 1(b). In this waveguide, light confinement is provided by total internal reflection at the core-cladding boundary. Air holes in the rings modify the dispersion in such a way as to match our requirements. Our choice of core material and PCF parameters has been dictated by two conditions, which cannot easily be simultaneously met. The first requirement is that there must be a relatively large refractive index contrast between core and cladding, so that the magnitude of the longitudinal component of the electric field becomes appreciable, and in turn that the mode profile changes strongly with frequency. The second requirement is that the holes should considerably modify the group velocity dispersion (GVD), in such a way that the maximum of the geometrical nonlinear coefficient is located inside the region of anomalous dispersion. However, the larger the refractive index contrast, the more the field is localized in the core, which makes the dispersion of the waveguide progressively more and more like that of a single rod surrounded by homogeneous silica, which has been proved to be nonoptimal in Ref. [3]. A trade-off between the above conditions must be found. We have examined the dispersion of many high-index glasses for the core material and systematically explored hundreds of specific parameters for the PCF cladding, but the above tellurite-based design seems to be one of the best solutions for our purposes. Such multiglass hybrid waveguides can be fabricated by using the pressure-cell approach [10].

For each frequency ω, the linear fundamental mode of the waveguide of Fig. 1(a) has a normalized electric field profile given by $\hat{\mathbf{e}}_\omega(\mathbf{r}_\perp)$, where $\mathbf{r}_\perp$ are the transverse coordinates. The inset in Fig. 1(a) shows a density plot of the *total* intensity $||\hat{\mathbf{e}}||^2 \equiv [\hat{e}_x^2 + \hat{e}_y^2 + \hat{e}_z^2]$ for the fiber parameters given in the caption, corresponding to our representative PCF NW design that we shall use throughout the Letter. Because of the specific symmetry of the PCF cladding under investigation, the waveguide does not exhibit any birefringence, and it has a fundamental mode that is degenerate in the two orthogonal polarization states. The crucial point of our formalism is that one can describe the full ω variations of $\hat{\mathbf{e}}$ through the Taylor series

$$\hat{\mathbf{e}}_\omega(\mathbf{r}_\perp) = \sum_{j\geq 0} \frac{1}{j!} \mathbf{f}_{\omega_0}^{(j)}(\mathbf{r}_\perp) \left(\frac{\Delta\omega}{\omega_0}\right)^j, \quad (1)$$

where $\Delta\omega \equiv \omega - \omega_0$ is the frequency detuning from an arbitrary reference frequency ω_0, and the quantity $\mathbf{f}_{\omega_0}^{(j)} \equiv [\omega_0^j \partial^j \hat{\mathbf{e}}_\omega(\mathbf{r}_\perp)/\partial\omega^j]_{\omega=\omega_0}$ is proportional to the jth frequency derivative of the mode profile. From now on, letters j, h, p, υ will be used for derivative indices. Following Ref. [3], one can rigorously prove that the equation governing the nonlinear light propagation of one of the two polarization states of the fundamental mode of the PCF NW is given by

$$i\partial_z Q + \hat{D}(i\partial_t)Q + \sum_{jhp\upsilon} \gamma^{jhp\upsilon} \hat{G}^j(i\partial_t)\phi^{hp\upsilon} = 0. \quad (2)$$

In Eq. (2), $Q(z, t)$ is the electric field envelope, $\hat{D}(i\partial_t) \equiv \beta(\omega_0 + i\partial_t) - \beta(\omega_0)$ is the dispersion operator that encodes all information on the fiber GVD around ω_0 [11], β is the ω-dependent propagation constant of the fundamental mode, and $\hat{G}^j(i\partial_t) \equiv [1 + (i/\omega_0)\partial_t][(i/\omega_0)\partial_t]^j$ is an operator that naturally contains the dynamics of the shock term at the zeroth order of the Taylor expansion ($j = 0$). The *convoluted nonlinear fields* used in Eq. (2) are defined as

$$\phi^{hp\upsilon}(z, t) \equiv \frac{[(i\partial_t)^h Q]\{R \otimes ([(i\partial_t)^p Q][(-i\partial_t)^\upsilon Q^*])\}}{\omega_0^{h+p+\upsilon}}, \quad (3)$$

where symbol $\otimes$ is used to denote a time convolution: $A \otimes B \equiv \int_{-\infty}^{+\infty} A(t - t')B(t')dt' = B \otimes A$. In Eq. (3), $R(t) \equiv (1 - \theta)\delta(t) + \theta h(t)$ is the nonlinear response function of the core, which is made of a tellurite glass following the design of Fig. 1(a), and includes the instantaneous Kerr [proportional to the Dirac delta $\delta(t)$] and the noninstantaneous Raman [proportional to $h(t)$] responses exhibited by the core material, θ being the relative importance between the two. In this Letter, from the experimental Raman gain of tellurite glass [solid blue line in Fig. 1(b), taken from Ref. [8]) we can extract a fit of $h(\omega)$ [dotted red line in Fig. 1(b)] that we thus use in the numerical simulations. The $\mathbf{r}_\perp$ dependence of $R(t)$ can be safely neglected, since most of the energy is located in the core material, which is also much more nonlinear than the surrounding silica cladding. Note that in Eq. (3), $\phi^{000} = Q \int R(t - t')|Q(t')|^2 dt'$ gives the conventional, zeroth order convolution that is used in the GNLSE, a widely used equation that is able to describe the propagation of nonlinear light with extreme accuracy in a large variety of physical situations [11,12].

The last ingredient in Eq. (2) contains the generalized nonlinear coefficients γ^{jhpv}, defined as

$$\gamma^{jhpv}(\omega_0) \equiv \frac{\omega_0}{16c}\int d\mathbf{r}_\perp \chi^{(3)}_{xxxx}(\mathbf{r}_\perp)\frac{\{[\mathbf{f}^{*(j)}_{\omega_0}\cdot\mathbf{f}^{(h)}_{\omega_0}][\mathbf{f}^{(p)}_{\omega_0}\cdot\mathbf{f}^{*(v)}_{\omega_0}]+[\mathbf{f}^{*(j)}_{\omega_0}\cdot\mathbf{f}^{(p)}_{\omega_0}][\mathbf{f}^{(h)}_{\omega_0}\cdot\mathbf{f}^{*(v)}_{\omega_0}]+[\mathbf{f}^{*(j)}_{\omega_0}\cdot\mathbf{f}^{*(v)}_{\omega_0}][\mathbf{f}^{(h)}_{\omega_0}\cdot\mathbf{f}^{(p)}_{\omega_0}]\}}{j!h!p!v!}, \quad (4)$$

where $\chi^{(3)}_{xxxx}(\mathbf{r}_\perp)$ is the third-order susceptibility, which is a function of the transverse coordinates in the waveguide of Fig. 1(a). Equation (4) is a generalization of the nonlinear coefficient commonly used in fiber optics [11], and takes into account the full vector nature of the field profile as well as its frequency variations. Such variations are at the very core of the new geometrical nonlinearities described here, since the Taylor series of Eq. (1) implies the existence of an infinite number of additional nonlinear terms that depend on progressively higher-order time derivatives of the envelope. The quantities γ^{jhpv} satisfy general symmetry relations that drastically reduce the number of independent nonlinear coefficients for each order of the derivative [3,13]: $\gamma^{jhpv}=\gamma^{vhpj}=\gamma^{jphv}=\gamma^{vphj}$, $\gamma^{jhhh}=\gamma^{hjhh}$, $\gamma^{jhhj}=\gamma^{hjjh}$. In Eqs. (1) and (3), each field derivative is associated with a factor ω_0^{-1}, which ensures convergence. Thus the physically meaningful nonlinear coefficients can be defined as $\tilde{\gamma}^{jhpv}\equiv\gamma^{jhpv}(\omega_0 t_0)^{-(j+h+p+v)}$, where t_0 is the input pulse duration.

From the expression in Eq. (4) one can define the zeroth order nonlinear coefficient of the waveguide $\gamma_0\equiv\gamma^{0000}=\tilde{\gamma}^{0000}$, corresponding to the conventional definition used in nonlinear fiber optics [11]. To first order in the Taylor expansion in Eq. (2) one can define the coefficient $\gamma_1\equiv\tilde{\gamma}^{1000}=\tilde{\gamma}^{0100}=\tilde{\gamma}^{0010}=\tilde{\gamma}^{0001}=\gamma^{1000}/(\omega_0 t_0)$, associated with nonlinear convoluted fields ϕ^{hpv} that contain only one time derivative of the envelope. Figure 2(a) shows plots of γ_0 and γ_1 versus reference wavelength for the fiber design of Fig. 1(a). The fiber GVD is shown in Fig. 2(b) with blue dots. It is clear from this figure the well-known fact that γ_0 decreases monotonically for longer wavelengths [14]. However, it is interesting to note that the geometrical nonlinear coefficient γ_1 initially increases, but then reaches a maximum near the infrared zero-GVD point of the fiber (located at $\lambda\simeq 2.4\ \mu$m), and then tends to zero for even longer wavelengths. The close vicinity of $\max(\gamma_1)$ to the anomalous GVD of the fiber is an atypical feature that we have found only in a few very specific designs, including the one presented in Fig. 1(a). The "normal" situation, which is also true for circular PNs surrounded by homogeneous media (such as, for instance, tapered fibers), is that $\max(\gamma_1)$ is located well within the region of normal GVD [3]. Some of previously published models take into account the frequency variation of the effective area in the scalar approximation as small variations of the shock time [15]. Such models fail to recognize that (i) polarization effects strongly modify the integrals in Eq. (4), and thus the scalar model is completely inadequate for the description of PCF-NWs, and (ii) expression of Eq. (1) must be intended more as a fit rather than a Taylor expansion, due to the fact that solitons continuously redshift along the nonlinear dispersion curve, so that all orders are important in the expansion, so that the shock time acquires a broadband dispersion that cannot be treated with the methods of Ref. [15].

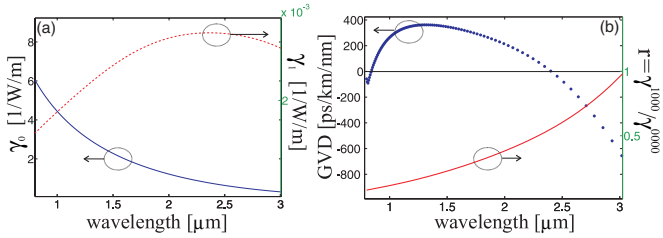

FIG. 2 (color online). Linear and nonlinear data for the PCF NW design of Fig. 1(a). (a) Blue solid and red dashed lines indicate, respectively, γ_0 and γ_1 versus wavelength. (b) Blue dots indicate the GVD of the waveguide, with zero-GVD points located at $\lambda\simeq 0.84\ \mu$m and $\lambda\simeq 2.4\ \mu$m. Red solid line indicates parameter $r=\gamma^{1000}/\gamma^{0000}$, that appears in Eq. (6).

We now show that the onset of geometrical nonlinearities leads to a strong suppression of the SSFS. In order to do this, we compare two direct numerical simulations of pulse propagation, the first one obtained by truncating the expansion of Eq. (2) to the zeroth order (one nonlinear convolution, corresponding to the conventional GNLSE) [Fig. 3(a)], the second one obtained by truncating the same sum to the second-order (15 nonlinear convolutions in total), which thus takes into account the dominant terms of the geometrical nonlinearities [Fig. 3(b)]. The density plots of Figs. 3(a) and 3(b) are constructed by joining

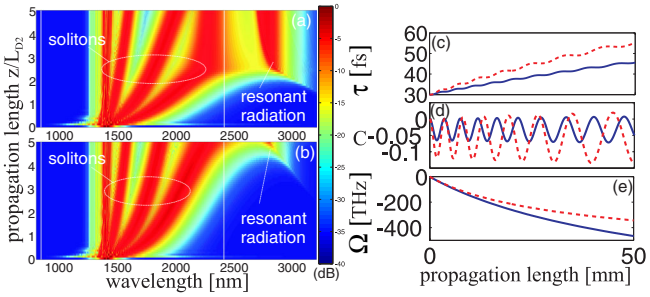

FIG. 3 (color online). (a) Density plot (in logarithmic color map with a 40 dB dynamic range density scale for intensities, as in Ref. [16]) showing nonlinear evolution of a $t_0=150$ fs, $P=1$ kW pulse in the waveguide of Fig. 1(a) according to Eq. (2) truncated at the 0th order, i.e., by using the conventional GNLSE. Second-order dispersion length is $L_{D2}\simeq 6$ cm. (b) Same as (a) but truncating Eq. (2) at the 2nd order. Vertical white lines indicate the two zero-GVD wavelengths. (c)–(e) z evolution of pulse duration τ [$t_0=\tau(0)=30$ fs], chirp C, and soliton frequency shift Ω according to Eqs. (5)–(7), for a $N=7$ soliton, pump wavelength $\lambda=1.4\ \mu$m. Blue solid (red dashed) line refers to the case $r=0$ ($r=0.2$) in Eqs. (5)–(7).

together hundreds of pulse spectra for discrete (but very close) steps in the propagation, analogously to what is done, e.g., in Fig. 3 of Ref. [16]. It is easily seen by comparing Fig. 3(a) with Fig. 3(b) that the net effect of the additional nonlinearities is to reduce considerably the SSFS in the fiber. Thus a unique interplay between the geometrical nonlinearities and the SSFS takes place in properly designed PCF NWs.

It is possible to qualitatively understand the reason of the above SSFS suppression mechanism by using the so-called moment method, that keep tracks of the solitonic parameters under the influence of small perturbations [11,17]. One assumes that after formation each solitonic pulse does not change its functional shape, given by $Q(t) = [Pt_0/\tau]^{1/2}\mathrm{sech}([t-T]/\tau)e^{-i\Omega(t-T)-iC(t-T)^2/(2\tau^2)}$, where T is the temporal delay of the solitonic pulse, Ω is its frequency detuning from the reference frequency ω_0, τ is the soliton pulse width, C is the pulse chirp, $\beta_2 = (\partial^2\beta/\partial\omega)_{\omega=\omega_0} < 0$ is the second-order (anomalous) dispersion coefficient, $P \equiv N^2P_0$ is the peak power, $P_0 \equiv |\beta_2|(t_0^2\gamma_0)^{-1}$ is the fundamental ($N = 1$) soliton power, N is the soliton order, and $T_R \equiv \int_{-\infty}^{+\infty} tR(t)dt$ is the first moment of the Raman response. One can prove that the z evolution of τ, C, and Ω is then given by the following closed set of equations:

$$\frac{d\tau}{dz} = \beta_2\frac{C}{\tau}, \tag{5}$$

$$\frac{dC}{dz} = \frac{4|\beta_2|N^2}{\pi^2 t_0\tau}\left[\left(1-\frac{t_0}{\tau}\right)+\frac{\Omega}{\omega_0}(1+4r)\right], \tag{6}$$

$$\frac{d\Omega}{dz} = -\frac{8T_RN^2|\beta_2|}{15t_0}\frac{1}{\tau^3}, \tag{7}$$

with the initial conditions $\tau(0) = t_0$, $C(0) = \Omega(0) = 0$. Higher-order terms in the dispersion and small terms proportional to C^2 have also been neglected for the sake of clarity. Geometrical nonlinearities are parametrized by the coefficient $r \equiv \gamma^{1000}/\gamma^{0000}$, the only one that appears in Eq. (6), shown in Fig. 2(b). Note that the condition $r > 1/4$ is necessary for the new nonlinearity to dominate the shock term in Eq. (6). Eqs. (5)–(7) are written under the simplifying assumption that the GVD does not change during the soliton evolution, and that the pulse duration is longer than 100 fs, so that one can use a well-known approximate expression for the Raman term [11]. The term on the right-hand side of Eq. (7), proportional to T_R, is responsible for the constant SSFS along the fiber [7,17]. The rate of this shift is very sensitive to the actual pulse width, since it is determined by τ^{-3}, and it is always directed towards negative detunings, i.e., towards the red part of the spectrum. However, due to the action of the right-hand side of Eq. (6), the soliton acquires a small chirp even if its initial chirp vanishes. The slope of this chirp is initially negative, due to the initial condition $\tau(0) = t_0$, which makes the term proportional to Ω/ω_0 dominant. Thus $C < 0$ in the initial stage of propagation, which in turn leads to a pulse broadening due to Eq. (5), for which $\beta_2 C > 0$. Finally, such broadening leads to a sharp suppression of the SSFS given by Eq. (7), due to the τ^{-3} dependence of its right-hand side. The long-term behavior of the propagation can only be understood by numerically solving Eqs. (5)–(7). In Figs. 3(c)–3(e) we show the z evolution of the quantities τ, C, and Ω for parameters given in the caption. C undergoes several deep oscillations, and its sign is mostly negative throughout the whole propagation [Fig. 3(d)]. The pulse duration τ undergoes similar oscillations (with a smaller magnitude), but overall it constantly grows [Fig. 3(c)]. Ω, however, is not too sensitive to such oscillations, due to the fact that its derivative never changes sign in Eq. (7) [Fig. 3(e)].

In conclusion, we have shown the emergence of a new type of nonlinearity in tellurite PNs embedded in a PCF cladding, which strongly depends on the geometrical parameters of the PCF design and the specific dispersion of the core material.

This work is supported by the German Max Planck Society for the Advancement of Science (MPG).

[1] J. Bures and R. Ghosh, J. Opt. Soc. Am. A **16**, 1992 (1999); L. Tong *et al.*, Nature (London) **426**, 816 (2003).
[2] M. A. Foster *et al.*, Opt. Express **16**, 1300 (2008).
[3] Tr. X. Tran and F. Biancalana, Opt. Express **17**, 17 934 (2009).
[4] S. Afshar V. and T. M. Monro, Opt. Express **17**, 2298 (2009); M. D. Turner, T. M. Monro, and S. Afshar V., Opt. Express **17**, 11 565 (2009).
[5] P. St. J. Russell, Science **299**, 358 (2003).
[6] N. A. Wolchover *et al.*, Opt. Express **15**, 829 (2007).
[7] F. M. Mitschke and L. F. Mollenauer, Opt. Lett. **11**, 659 (1986); J. P. Gordon, Opt. Lett. **11**, 662 (1986).
[8] M. D. O'Donnell *et al.*, J. Am. Ceram. Soc. **90**, 1448 (2007).
[9] R. A. H. El-Mallawany, *Tellurite Glasses Handbook: Physical Properties And Data* (CRC, Boca Raton, FL, 2002).
[10] M. A. Schmidt *et al.*, Opt. Lett. **34**, 1946 (2009).
[11] G. P. Agrawal, *Nonlinear Fiber Optics* (Academic, San Diego, 2007), 4th ed.
[12] A. L. Gaeta, Opt. Lett. **27**, 924 (2002).
[13] F. Poletti and P. Horak, J. Opt. Soc. Am. B **25**, 1645 (2008).
[14] B. Kibler, J. M. Dudley, and S. Coen, Appl. Phys. B **81**, 337 (2005).
[15] K. J. Blow and D. Wood, IEEE J. Quantum Electron. **25**, 2665 (1989); N. Karasawa *et al.*, IEEE J. Quantum Electron. **37**, 398 (2001).
[16] J. M. Dudley, G. Genty, and S. Coen, Rev. Mod. Phys. **78**, 1135 (2006).
[17] J. Santhanam and G. P. Agrawal, Opt. Commun. **222**, 413 (2003).